

Band-filling and correlation controlling electronic properties and magnetism in $K_xFe_{2-y}Se_2$: A slave boson study

Da-Yong Liu¹, Ya-Min Quan¹, Xiao-Jun Zheng¹, Xiang-Long Yu¹, Liang-Jian Zou^{1,a}

¹ *Key Laboratory of Materials Physics,
Institute of Solid State Physics,
Chinese Academy of Sciences,
P. O. Box 1129, Hefei 230031,
People's Republic of China*

(Dated: October 16, 2012)

Abstract

In this paper we investigate the electronic and magnetic properties of $K_xFe_{2-y}Se_2$ materials at different band fillings utilizing the multi-orbital Kotliar-Ruckenstein's slave-boson mean field approach. We find that at three-quarter filling, corresponding to KFe_2Se_2 , the ground state is a paramagnetic bad metal. Through band renormalization analysis and comparison with the angle-resolved photoemission spectra data, we identify that KFe_2Se_2 is also an intermediate correlated system, similar to iron-pnictide systems. At two-third filling, corresponding to the Fe^{2+} -based systems, the ground state is a striped antiferromagnetic (SAFM) metal with spin density wave gap partially opened near the Fermi level. In comparison, at half filling case, corresponding to the Fe^{3+} -based compounds, besides SAFM, a *Néel* antiferromagnetic metallic ground state without orbital ordering is observed in the intermediate correlation range, and an orbital selective Mott phase (OSMP) accompanied with an intermediate-spin to high-spin transition is also found. These results demonstrate that the band filling and correlation control the electronic state, Fermi surface topology and magnetism in $K_xFe_{2-y}Se_2$.

PACS numbers: 74.70.Xa, 71.27.+a, 71.10.-w

I. INTRODUCTION

Recently a new iron selenide superconductor $K_xFe_{2-y}Se_2$ with T_c above 30 K [1] has attracted considerable attention for its unique high *Néel* transition temperature and insulating properties, as well as the presence of intrinsic Fe-vacancy ordering [2–5], quite different from the other iron-based superconducting materials. These unusual properties arise an assumption that $K_xFe_{2-y}Se_2$ may be a strongly correlated system. KFe_2Se_2 is isostructural to the 122 system, *e.g.* $BaFe_2As_2$, but chemically is close to $FeSe$. On average there are 6.5 electrons with equal ratio of Fe^{2+} and Fe^+ in KFe_2Se_2 , rather than 6 ones in the iron-pnictide parent compounds with solely Fe^{2+} . Therefore it can be regarded as an electron overdoped 11 system, in contrast to the underdoped KFe_2As_2 which has 5.5 electrons with equal ratio of Fe^{2+} and Fe^{3+} , and $FeAs$ which has 5 ones with Fe^{3+} . As a consequence, only the electron Fermi surface (FS) pockets exist around the M points in KFe_2Se_2 , as observed in recent angle-resolved photoemission spectroscopy (ARPES) experiments [6, 7] and in electronic structure calculations [8, 9]. Thus, the FS nesting between the hole pocket around the Γ point and the electron pocket around the M point, which widely exists in $FeAs$ -based materials, is absent in KFe_2Se_2 compound.

Due to its unique electronic structure properties, the magnetic properties of $K_xFe_{2-y}Se_2$ are focused on. Because of the difficulty of single crystal preparation for pure AFe_2Se_2 ($A=K, Tl, Rb$, or Cs), its magnetic properties are mainly studied theoretically, but still a debating issue, as addressed in what follows: the local density approximation (LDA) calculations suggested that KFe_2Se_2 is a striped antiferromagnetic (SAFM) order, same to the 1111 and 122 phases of the $FeAs$ -based materials [9]; while some others [8] thought it to be bi-collinear AFM with $(\pi/2, \pi/2)$ wave-vector, similar to $FeTe$ [10]. However, the LDA calculations suggested that $TlFe_2Se_2$ is a checkerboard AFM (π, π) order [11], and the dynamical spin susceptibility obtained within random phase approximation (RPA) also suggested the (π, π) instability in KFe_2Se_2 [12, 13]. These discrepant results show that further investigations on the magnetism are deserved to understand the unique properties in AFe_2Se_2 ($A=K, Tl, Rb$, or Cs) compounds.

Many recent experiments [14–20] reported the wide existence of the phase separation in $K_xFe_{2-y}Se_2$ materials. A scanning tunneling spectroscopy (STS) experiment demonstrated the phase-separated component KFe_2Se_2 is the parent phase contributing to the superconductivity, and $K_{0.8}Fe_{1.6}Se_2$ component is an Fe-vacancy order insulator [14], implying that pure KFe_2Se_2 in the normal state is more possibly a paramagnetic (PM) phase. One may notice that different

K contents in $K_x\text{Fe}_{2-y}\text{Se}_2$ lead to different band fillings of Fe 3d orbitals, hence to quite different electronic and magnetic properties. Further Chen *et al.* reported that the electronic states and magnetic phase diagrams of $K_x\text{Fe}_{2-y}\text{Se}_2$ system are closely connected with the Fe valences [15]. We also notice that various theoretical magnetic configurations obtained within the first-principles calculations for AFe_2Se_2 (A=K, Tl, Rb, or Cs) do not include the Coulomb correlation correction [8, 9, 11], which implies a weak electronic correlation in AFe_2Se_2 , in contrast with the intermediate electronic correlation in the FeAs-based compounds [21]. Thus a few of questions are urgent to be answered: what is the realistic electron filling ? Moreover how does the band filling affect the electronic properties and magnetism in $K_x\text{Fe}_{2-y}\text{Se}_2$? Considering that KFe_2Se_2 is a possible parent phase of superconducting state, we will focus on $K_x\text{Fe}_{2-y}\text{Se}_2$ system in the absence of ordered Fe vacancy at various electron fillings throughout this paper.

In this paper, to uncover the role of electronic correlation on the groundstate properties of AFe_2Se_2 , we adopt Kotliar-Ruckenstein's slave boson (KRSB) mean field approach [21–23] to study the magnetic and electronic properties at different band fillings in K-doped iron selenides. Based on our previous LDA calculation results [12], we first present an effective three-orbital model for KFe_2Se_2 , and then determine the ground states of this model at different electron fillings. We show that the ground state of $K_x\text{Fe}_{2-y}\text{Se}_2$ at fillings of 3/4, 2/3 and a half is a PM metallic phase, a SAFM with orbital ordering, and a *Néel* AFM one without orbital ordering in the intermediate and strong correlation regimes in addition to an orbital selective Mott phase (OSMP) related with an intermediate-spin to high-spin transition, respectively, showing that the band filling controls not only the FS topology, but also the electronic structure and magnetic properties of Fe-based superconducting materials. The rest of this paper is organized as follows: a three-orbital tight-binding model and the multi-orbital slave-boson mean-field approach are presented in *Sec. II*; the numerical results and discussions are shown in *Sec. III*; the last section is devoted to the remarks and summary.

II. THREE-ORBITAL TIGHT-BINDING MODEL AND SLAVE BOSON APPROACH

Based on our previous electronic structure calculations [12], we find that FS is mainly contributed by three t_{2g} orbitals, thus the system can be described by a three-orbital model, similar to iron pnictides [24–27]. We extract an effective three-orbital tight-binding model from our LDA band structures. The tight-binding model Hamiltonian for the three-orbital model in the momen-

tum space is described as,

$$H_0 = \sum_{k,\alpha,\beta,\sigma} (\epsilon_\alpha \delta_{\alpha\beta} + T^{\alpha\beta}(\mathbf{k})) C_{k\alpha\sigma}^\dagger C_{k\beta\sigma} - \mu \sum_{k\alpha\sigma} n_{k\alpha\sigma}, \quad (1)$$

where $T^{\alpha\beta}(\mathbf{k})$ is the kinetic energy term, ϵ_α denotes the on-site energy of the α orbital, and μ is the chemical potential determined by the electron filling. The three-orbital tight-binding fitting of the Fe-3d bands is displayed in the solid lines, in comparison with the original five bands [12] in the dot lines, as shown in Fig. 1. It is obviously found that the band structures in KFe_2Se_2 are similar to that of LaFeAsO [28], only the position of Fermi energy E_F is shifted. Therefore this model can describe both the FeSe-based and FeAs-based systems through changing the chemical potential.

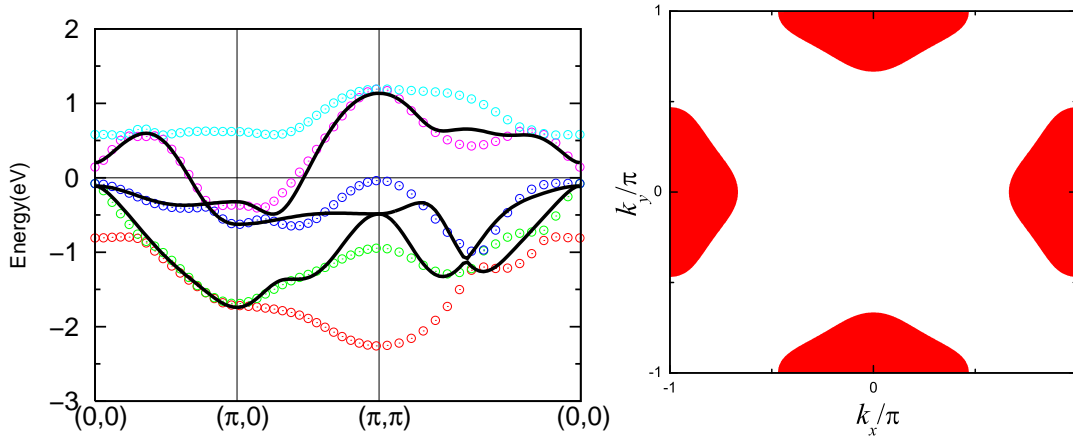


FIG. 1. (Color online) Left panel: the band structures of the Fe-3d orbitals obtained by the LDA and its three-orbital tight-binding fitting. Dot lines are the LDA five bands [12], and solid lines the fitted effective three bands. Right panel: the corresponding Fermi surface for parent material KFe_2Se_2 at the first Brillouin zone obtained by the three-orbital tight-binding model.

The tight-binding parameters of the three-orbital model for KFe_2Se_2 are listed in the following. The on-site energies measured from the Fermi energy for the three orbitals are $(\epsilon_1, \epsilon_2, \epsilon_3) = (-511.92, -511.92, -341.63)$, respectively, in units of meV. Here orbital indices (1, 2, 3) indicate the d_{xz} , d_{yz} , and d_{xy} components, respectively. Similar to BaFe_2As_2 [29], the orbital-dependent kinetic energy matrix elements are expressed in terms of the inter-orbital and intra-orbital hopping

integrals as follows,

$$\begin{aligned}
T^{11/22} &= 2t_{x/y}^{11} \cos k_x + 2t_{y/x}^{11} \cos k_y + 4t_{xy}^{11} \cos k_x \cos k_y \\
&\quad \pm 2t_{xx}^{11} (\cos 2k_x - \cos 2k_y) + 4t_{xxy/xyy}^{11} \cos 2k_x \cos k_y \\
&\quad + 4t_{xyy/xyx}^{11} \cos 2k_y \cos k_x + 4t_{xxyy}^{11} \cos 2k_x \cos 2k_y, \\
T^{33} &= 2t_x^{33} (\cos k_x + \cos k_y) + 4t_{xy}^{33} \cos k_x \cos k_y + 2t_{xx}^{33} (\cos 2k_x + \cos 2k_y) \\
&\quad + 4t_{xxy}^{33} (\cos 2k_x \cos k_y + \cos 2k_y \cos k_x) + 4t_{xxyy}^{33} \cos 2k_x \cos 2k_y, \\
T^{12} &= 4t_{xy}^{12} \sin k_x \sin k_y + 4t_{xxy}^{12} (\sin 2k_x \sin k_y + \sin 2k_y \sin k_x) \\
&\quad + 4t_{xxyy}^{12} \sin 2k_x \sin 2k_y, \\
T^{13/23} &= \pm 2it_x^{13} \sin k_{x/y} \pm 4it_{xy}^{13} \cos k_{y/x} \sin k_{x/y} \\
&\quad \pm 4it_{xxy}^{13} \cos k_{y/x} \sin 2k_{x/y},
\end{aligned}$$

The intra-orbital and inter-orbital hopping parameters up to the fifth nearest-neighbor for the fitting of the three-band structure in Fig. 1 are shown in Table I.

TABLE I. The nonzero matrix elements of intra-orbital $t_i^{\alpha\alpha}$ and inter-orbital $t_i^{\alpha\beta}$ hopping parameters up to fifth neighbors of the three-orbital tight-binding model through fitting the band structures. All the parameters are in units of meV.

$t_i^{\alpha\alpha}$	$i = x$	$i = y$	$i = xy$	$i = xx$	$i = xxy$	$i = xyy$	$i = xxyy$
$\alpha = 1/2$	60.87	77.65	21.83	54.35	-34.35	11.97	31.67
$\alpha = 3$	-53.39		301.2	21.61	-31.6		-70.04
$t_i^{\alpha\beta}$	$i = x$	$i = xy$	$i = xxy$	$i = xxyy$			
$\alpha\beta = 12$		-119.57	50.99	-12.55			
$\alpha\beta = 13/23$	302.39	122.5	-14.64				

Considering the Coulomb interaction, in addition to the kinetic term in Eq. (1), we describe the electronic interaction part of the multi-orbital Hamiltonian as follows,

$$\begin{aligned}
H_I &= U \sum_{i,\alpha} n_{i\alpha\uparrow} n_{i\alpha\downarrow} + U' \sum_{\substack{i \\ \alpha \neq \beta}} n_{i\alpha\uparrow} n_{i\beta\downarrow} + (U' - J_H) \sum_{\substack{i,\sigma \\ \alpha < \beta}} n_{i\alpha\sigma} n_{i\beta\sigma} \\
&\quad - J_H \sum_{\substack{i \\ \alpha \neq \beta}} C_{i\alpha\uparrow}^\dagger C_{i\alpha\downarrow} C_{i\beta\downarrow}^\dagger C_{i\beta\uparrow} + J_H \sum_{\substack{i \\ \alpha \neq \beta}} C_{i\alpha\uparrow}^\dagger C_{i\alpha\downarrow}^\dagger C_{i\beta\downarrow} C_{i\beta\uparrow}
\end{aligned} \tag{2}$$

where $U(U')$ denotes the intra-(inter-)orbital Coulomb repulsion interaction and J_H the Hund's rule coupling. Considering the rotation symmetry of the system, we adopt $U' = U - 2J_H$.

We notice that in FeAs-based materials, the electronic filling for the present three-orbital model is only at two-third filling, *i.e.* $n=4$, the correct FS can be reproduced [26–28]. In KFe_2Se_2 compound, the Fe ions have two kinds of valence, Fe^{2+} and Fe^+ with equal ratio, and the average electron number is 6.5 per site, different from Fe^{2+} with 6 electrons in FeAs-based parent materials. Consequently, pure KFe_2Se_2 should be at a filling of three quarters (*i.e.* $n=4.5$) at which the FS can be reproduced correctly in the present three-orbital model. The obtained FS of KFe_2Se_2 is plotted at $k_z=0$ in Fig. 1, with four electron-like FS pockets. The hole-like FS pockets at Γ are absent. Such a FS topology is in agreement with the recent ARPES experiments [6, 7] and the band structure calculations [8, 9]. To explore the band filling dependence of the electronic state, we also extend the band filling to 2/3 and half, which corresponds to the Fe^{2+} and Fe^{3+} systems, respectively.

KRSB mean field approach is known as one of the effective methods to treat the wide electronic correlation in the many-body systems. Here, we extend the single-orbital KRSB mean-field method to the multi-orbital situation [21, 23] and apply it on $\text{K}_x\text{Fe}_{2-y}\text{Se}_2$. We introduce new fermion operators $f_{i\alpha\sigma}$ slaved by boson operators e_i , $p_{i\alpha\sigma}$, $d_{i\alpha\sigma\beta\sigma_\gamma}$, $b_{i\alpha}$, $t_{i\alpha\beta\sigma}$, $r_{i\sigma_\alpha\sigma_\beta\sigma_\gamma}$, $q_{i\alpha}$, $u_{i\alpha\sigma\beta\sigma_\gamma}$, $v_{i\alpha\sigma}$ and s_i , which represent the empty, single occupation with α orbital and σ spin, double occupation with β orbital spin σ_β and γ orbital spin σ_γ , double occupation with two electrons in orbital α , triplicate occupation with two electrons in orbital α and one electron in orbital β with spin σ , triplicate occupation with each electron in orbital α , β and γ with spin σ_α , σ_β , and σ_γ , quaternary occupation with two electrons in orbital β and γ , quaternary occupation with two electrons in orbital α , one electron in orbital β with spin σ_β and one electron in orbital γ with spin σ_γ , fivefold occupation with four electrons in orbitals β and γ , and one electron in orbital α with spin σ , and sixfold occupation, respectively.

The completeness of these boson fields gives rise to the normalization condition as follows:

$$\begin{aligned}
e_i^\dagger e_i + \sum_{\alpha,\sigma} p_{i\alpha\sigma}^\dagger p_{i\alpha\sigma} + \sum_{\alpha} b_{i\alpha}^\dagger b_{i\alpha} + \sum_{\alpha,\sigma_\beta,\sigma_\gamma} d_{i\alpha\sigma\beta\sigma_\gamma}^\dagger d_{i\alpha\sigma\beta\sigma_\gamma} + \sum_{\sigma_\alpha,\sigma_\beta,\sigma_\gamma} r_{i\sigma_\alpha\sigma_\beta\sigma_\gamma}^\dagger r_{i\sigma_\alpha\sigma_\beta\sigma_\gamma} \\
+ \sum_{\alpha,\beta,\sigma} t_{i\alpha\beta\sigma}^\dagger t_{i\alpha\beta\sigma} + \sum_{\alpha} q_{i\alpha}^\dagger q_{i\alpha} + \sum_{\alpha,\sigma,\sigma_\beta,\sigma_\gamma} u_{i\alpha\sigma\beta\sigma_\gamma}^\dagger u_{i\alpha\sigma\beta\sigma_\gamma} + \sum_{\alpha,\sigma} v_{i\alpha\sigma}^\dagger v_{i\alpha\sigma} + s_i^\dagger s_i = 1
\end{aligned} \quad (3)$$

Projecting the original Hamiltonian Eqs. (1) and (2) into the new slave-boson representation, the

multi-orbital Hubbard model Hamiltonian is described as:

$$\begin{aligned}
H = & \sum_{i,j,\alpha,\beta,\sigma} t_{\alpha\beta}^{ij} Z_{i\alpha\sigma}^\dagger Z_{j\beta\sigma} f_{i\alpha\sigma}^\dagger f_{j\beta\sigma} + \sum_{i\alpha\sigma} (\epsilon_\alpha - \mu) f_{i\alpha\sigma}^\dagger f_{i\alpha\sigma} + U \sum_{i,\alpha} b_{i\alpha}^\dagger b_{i\alpha} + J_H \sum_{i,\alpha}^{\alpha,\beta,\gamma} (b_{i\beta}^\dagger b_{i\gamma} + b_{i\gamma}^\dagger b_{i\beta}) \\
& + (U' - J_H) \sum_{i,\alpha,\sigma} d_{i\alpha\sigma\bar{\sigma}}^\dagger d_{i\alpha\sigma\bar{\sigma}} + U' \sum_{i,\alpha,\sigma} d_{i\alpha\sigma\bar{\sigma}}^\dagger d_{i\alpha\sigma\bar{\sigma}} + (U + 2U' - J_H) \sum_{i,\alpha,\sigma}^{\alpha,\beta,\gamma} (t_{i\beta\gamma\sigma}^\dagger t_{i\beta\gamma\sigma} + t_{i\gamma\beta\sigma}^\dagger t_{i\gamma\beta\sigma}) \\
& + J_H \sum_{i,\alpha,\sigma}^{\alpha,\beta,\gamma} (t_{i\beta\alpha\sigma}^\dagger t_{i\gamma\alpha\sigma} + t_{i\beta\alpha\sigma}^\dagger t_{i\gamma\alpha\sigma}) + 3(U' - J_H) \sum_{i,\sigma} r_{i\sigma\alpha\sigma_\beta\sigma_\gamma}^\dagger r_{i\sigma\alpha\sigma_\beta\sigma_\gamma} \\
& + (3U' - J_H) \sum_{i,\alpha,\sigma}^{\alpha,\beta,\gamma} r_{i\sigma\alpha\sigma_\beta\sigma_\gamma}^\dagger r_{i\sigma\alpha\sigma_\beta\sigma_\gamma} + 2(U + 2U' - J_H) \sum_{i,\alpha} q_{i\alpha}^\dagger q_{i\alpha} + J_H \sum_{i,\alpha}^{\alpha,\beta,\gamma} (q_{i\beta}^\dagger q_{i\gamma} + q_{i\gamma}^\dagger q_{i\beta}) \\
& + (U + 5U' - 3J_H) \sum_{i,\alpha,\sigma}^{\alpha,\beta,\gamma} u_{i\alpha\sigma\beta\sigma_\gamma}^\dagger u_{i\alpha\sigma\beta\sigma_\gamma} + (U + 5U' - 2J_H) \sum_{i,\alpha,\sigma}^{\alpha,\beta,\gamma} u_{i\alpha\sigma\beta\sigma_\gamma}^\dagger u_{i\alpha\sigma\beta\sigma_\gamma} \\
& + (2U + 8U' - 4J_H) \sum_{i,\alpha,\sigma} v_{i\alpha\sigma}^\dagger v_{i\alpha\sigma} + (3U + 12U' - 6J_H) \sum_i s_i^\dagger s_i
\end{aligned} \tag{4}$$

where the renormalization factor

$$Z_{i\alpha\sigma} = (1 - \tilde{Q}_{i\alpha\sigma})^{-\frac{1}{2}} \tilde{Z}_{i\alpha\sigma} \tilde{Q}_{i\alpha\sigma}^{-\frac{1}{2}} \tag{5}$$

$$\begin{aligned}
\tilde{Z}_{i\alpha\sigma} = & e_i^\dagger p_{i\alpha\sigma} + p_{i\alpha\bar{\sigma}}^\dagger b_{i\alpha} + \sum_{\sigma'}^{\alpha,\beta,\gamma} p_{i\beta\sigma'}^\dagger d_{i\gamma\sigma\sigma'} + \sum_{\sigma'}^{\alpha,\beta,\gamma} p_{i\gamma\sigma'}^\dagger d_{i\beta\sigma'\sigma} + \sum_{\beta}^{\beta \neq \alpha} b_{i\beta}^\dagger t_{i\beta\alpha\sigma} \\
& + \sum_{\sigma',\sigma''}^{\alpha,\beta,\gamma} d_{i\alpha\sigma\beta\sigma_\gamma}^\dagger r_{i\sigma\alpha\sigma_\beta\sigma_\gamma} + \sum_{\sigma'}^{\alpha,\beta,\gamma} d_{i\gamma\bar{\sigma}\sigma'}^\dagger t_{i\alpha\beta\sigma'} + \sum_{\sigma'}^{\alpha,\beta,\gamma} d_{i\beta\sigma'\bar{\sigma}}^\dagger t_{i\alpha\gamma\sigma'} + \sum_{\sigma',\sigma''} r_{i\bar{\sigma}\alpha\sigma_\beta\sigma_\gamma}^\dagger u_{i\alpha\sigma\beta\sigma_\gamma} \\
& + t_{i\gamma\alpha\bar{\sigma}}^\dagger q_{i\beta} + t_{i\beta\alpha\bar{\sigma}}^\dagger q_{i\gamma} + \sum_{\sigma'} t_{i\gamma\beta\sigma'}^\dagger u_{i\gamma\sigma\alpha\sigma_\beta} + \sum_{\sigma'} t_{i\beta\gamma\sigma'}^\dagger u_{i\beta\sigma_\gamma\sigma_\alpha} + q_{i\alpha}^\dagger v_{i\alpha\sigma} \\
& + \sum_{\sigma'} u_{i\gamma\bar{\sigma}\alpha\bar{\sigma}_\beta}^\dagger v_{i\beta\bar{\sigma}} + \sum_{\sigma'} u_{i\beta\sigma_\gamma\bar{\sigma}_\alpha}^\dagger v_{i\gamma\sigma'} + v_{i\alpha\bar{\sigma}}^\dagger s_i
\end{aligned} \tag{6}$$

The corresponding Fermion number constraint for α orbital with spin σ reads:

$$\tilde{Q}_{i\alpha\sigma} = f_{i\alpha\sigma}^\dagger f_{i\alpha\sigma} \tag{7}$$

where

$$\begin{aligned}
\tilde{Q}_{i\alpha\sigma} = & p_{i\alpha\sigma}^\dagger p_{i\alpha\sigma} + b_{i\alpha}^\dagger b_{i\alpha} + \sum_{\sigma'} d_{i\beta\sigma_\gamma\sigma_\alpha}^\dagger d_{i\beta\sigma_\gamma\sigma_\alpha} + \sum_{\sigma'} d_{i\gamma\sigma_\alpha\sigma_\beta}^\dagger d_{i\gamma\sigma_\alpha\sigma_\beta} + \sum_{\sigma',\sigma''} r_{i\sigma\alpha\sigma_\beta\sigma_\gamma}^\dagger r_{i\sigma\alpha\sigma_\beta\sigma_\gamma} \\
& + \sum_{\beta,\sigma} t_{i\alpha\beta\sigma}^\dagger t_{i\alpha\beta\sigma} + \sum_{\beta} t_{i\beta\alpha\sigma}^\dagger t_{i\beta\alpha\sigma} + \sum_{\beta}^{\beta \neq \alpha} q_{i\beta}^\dagger q_{i\beta} + \sum_{\sigma'} u_{i\gamma\sigma_\alpha\sigma_\beta}^\dagger u_{i\gamma\sigma_\alpha\sigma_\beta} + \sum_{\sigma'} u_{i\beta\sigma_\gamma\sigma_\alpha}^\dagger u_{i\beta\sigma_\gamma\sigma_\alpha} \\
& + \sum_{\sigma',\sigma''} u_{i\alpha\sigma\beta\sigma_\gamma}^\dagger u_{i\alpha\sigma\beta\sigma_\gamma} + \sum_{\beta\sigma}^{\beta \neq \alpha} v_{i\beta\sigma}^\dagger v_{i\beta\sigma} + v_{i\alpha\sigma}^\dagger v_{i\alpha\sigma} + s_i^\dagger s_i
\end{aligned} \tag{8}$$

Averaging the boson operators in Eq.(4)-(8), we can obtain an effective mean field Hamiltonian, hence the total ground-state energy. The original fermions are guaranteed by the constraints Eq.(7), which are implemented by means of the corresponding generalized Lagrange multiplier method. In order to determine the stable magnetic ground state, we minimize the total energies for different magnetic configurations based on the pattern search method. To simplify the calculations, various symmetries should be utilized. For instance, in the AFM situation with two sublattices, the single occupation probabilities $p_{\alpha\uparrow}^B$ in sublattice B are identical to $p_{\alpha\downarrow}^A$ in sublattice A , double occupation probabilities $d_{\alpha\downarrow}^B = d_{\alpha\uparrow}^A$, etc..

III. RESULTS AND DISCUSSIONS

In this section, we present main numerical results on the electronic and magnetic properties within the three-orbital model for iron selenide systems. The fillings of three quarters and two thirds, as well as half-filling, are all considered for comparison.

A. Three-quarter filling case

We firstly consider the electron filling $n=4.5$ case, corresponding to pure KFe_2Se_2 compounds. Note that we adopt the hole representation for convenience within KRSB mean field approach throughout this paper. Thus the particle number at the three-quarter filling case is 1.5 within the three-orbital model. Taking into account several types of magnetic configurations with high symmetry, the PM, ferromagnetic (FM), *Néel* AFM and SAFM cases, we find that only the PM phase is the most stable at a filling of three quarters when U increases from 0 up to 5 eV. Because of the mixing valence of Fe^{2+} and Fe^+ in KFe_2Se_2 , the system is not a magnetic ordered and insulating state in the homogenous phase. Since the electron fillings of both Fe^{2+} and Fe^+ are away from half filling, unlike mixing valent $\text{Na}_{0.5}\text{CoO}_2$ [30], KFe_2Se_2 does not form charge ordering. Previous work on charge susceptibility shows that the Coulomb interaction suppresses the charge instability [12, 31], thus it is hard to form charge ordering in KFe_2Se_2 .

Within the present KRSB framework, the dependence of various boson occupancies on the Coulomb interaction U at $J_H=0.25U$ is plotted in Fig. 2. It is clearly found that the empty occupation e , single occupation p_3 and double occupation b_3 with orbital xy are dominant for small U . With the increase of the Coulomb interaction, the empty occupation e and triple occupation

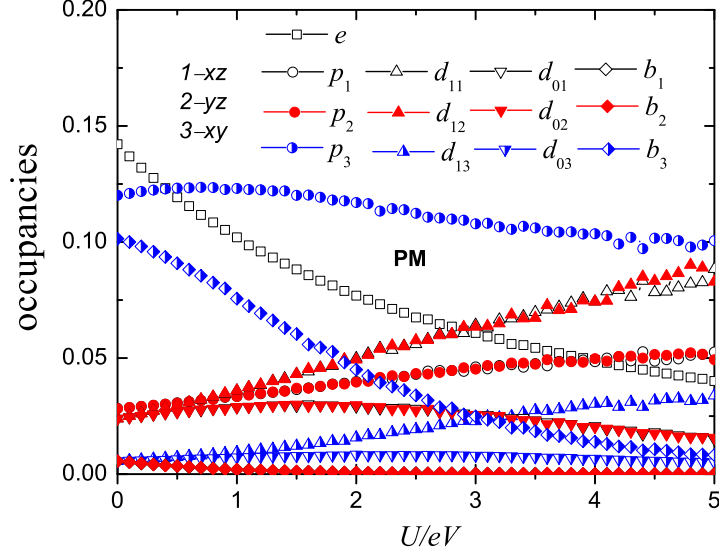


FIG. 2. Dependence of boson occupancies on Coulomb interaction U at an electron filling of $n=4.5$, and $J_H=0.25U$. Note that in the PM case, $d_{0\alpha} = d_{\alpha\uparrow\downarrow} = d_{\alpha\downarrow\uparrow}$, $d_{1\alpha} = d_{\alpha\uparrow\uparrow} = d_{\alpha\downarrow\downarrow}$.

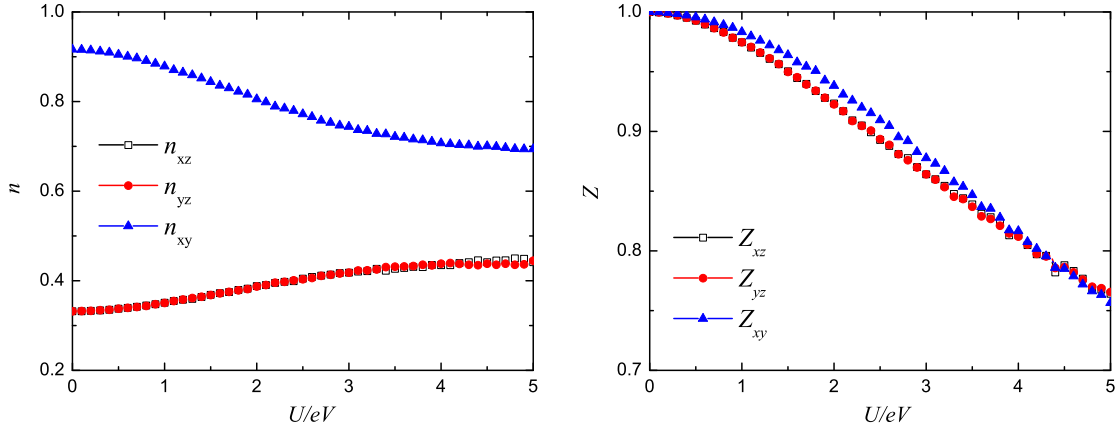


FIG. 3. (Color online) Orbital occupations (left panel), and renormalization factor (right panel) as a function of the Coulomb interaction U at $n=4.5$, and $J_H=0.25U$.

b_3 decrease sharply, while d_{11} , d_{12} and d_{13} ($d_{1\alpha} = d_{\alpha\uparrow\uparrow} = d_{\alpha\downarrow\downarrow}$) increase due to the increasing of the Hund's rule coupling and the Coulomb interaction. This shows that the system is a PM and the magnetic moment of each Fe spin increases with the lift of U and J_H , rather than a nonmagnetic one.

The orbital occupations as a function of the Coulomb interaction are given in the left panel of Fig. 3. It is obviously found that the electrons are occupied at the lower energy xz - and yz -

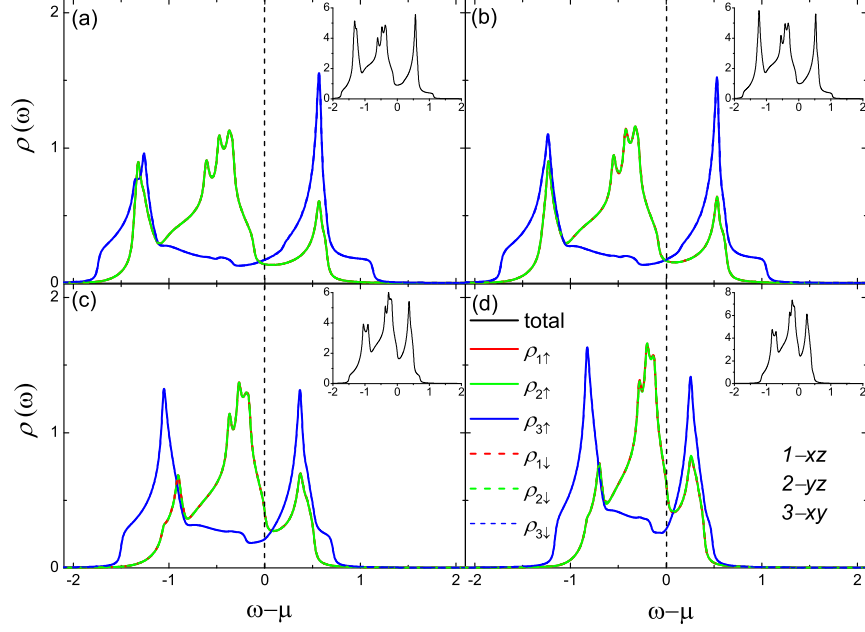


FIG. 4. Projected densities of states are plotted for $U=0$ (a), 1.0 eV (b), 3.0 eV (c), and 5.0 eV (d) at $n=4.5$, respectively, with $J_H=0.25U$. Inset: total densities of states.

orbitals. And there is no orbital polarization between the xz - and yz -orbitals. With the increase of Coulomb interaction, a fraction of electrons in the xz - and yz -orbitals transfer to higher energy xy -orbital since larger J_H enhances the effect of the Hund's rule. Thus the high energy xy orbital occupies more electrons as J_H increases. The renormalization factors of each orbital as a function of the Coulomb interaction U are shown in the right panel of Fig. 3. With the increase of Coulomb interaction, the bandwidths of the three orbitals become narrower and narrower, and the renormalization factors become small. We notice that in the PM phase, the degeneracy of orbital xz and yz is not removed, and the renormalization factors of bandwidths in different orbitals are nearly the same. When U is 3, 4 and 5 eV, the renormalization factor Z is about 0.85, 0.8 and 0.76, respectively, giving rise to the band mass of original fermions $m_b/m = 1/Z^2 \sim 1.38, 1.56$ and 1.73, respectively, and yielding a mass renormalization factor of about 2 at $U=5$ eV. We expect that the disorder effect and the spin fluctuations beyond the KRSB mean field approximation will further narrow the bandwidths and enhance the effective mass. This band narrowing factor is comparable with the experimental ones from ARPES [32] and de Haas-Van Alphen [33], indicating that KFe_2Se_2 lies in the intermediate correlation region, similar to the FeAs-based systems. While in the presence of the Fe-vacancy, the measured renormalization factor is about 6.1 in $(\text{Ti,Rb})_x\text{Fe}_{2-y}\text{Se}_2$, greatly larger than 2. This shows that most probably the insulating proper-

ties in $K_xFe_{2-y}Se_2$ systems are induced by the ordering of Fe vacancies, rather than by the strong electronic correlation.

The projected densities of states (PDOS) of KFe_2Se_2 for the Coulomb interaction $U=0, 1, 3$ and 5 eV are shown in Fig. 4. The finite DOS at FS shows a pseudo-gap-like structure, and there is no obvious van Hove singularity. Nevertheless in FeAs-based compounds, a considerable van Hove singularities in the DOS is attributed to the FS nesting with wave vector $\mathbf{Q}=(\pi, 0)$ [34]. Therefore, the absence of the van Hove singularities in the DOS of KFe_2Se_2 may be the consequence of the breakdown of the FS nesting, which arises from the fact that there lacks the hole pockets around Γ point. With the increase of the Coulomb interaction from 0 to 5 eV, the bandwidth becomes narrow, $W \sim 2.5$ eV at $U=3$ eV, smaller than 3.2 eV at $U=0$, showing that the system is a correlated bad metal and is in the intermediate correlation region with $W \sim U$.

Through the analysis above, we find that at 3/4 filling, the $K_xFe_{2-y}Se_2$ system, corresponding to KFe_2Se_2 , is a PM phase. We also clarify that KFe_2Se_2 lies in intermediate correlation region, similar to the FeAs-based compounds.

B. Two-third filling case

On the other hand, the electron filling at $n=4$ corresponds to Fe^{2+} -based compounds, such as FeSe and LaFeAsO, *etc.*. The dependence of boson occupancy probabilities on the Coulomb interaction is also shown in Fig. 5. Comparing with $n=4.5$ case, we find that with the increase of U , the system transits from a PM metallic phase to a SAFM metallic one at a critical point $U_c \approx 1.2$ eV. In the PM phase, the single occupations in the xy -orbital p_3 and empty occupancy e are dominant. Other multiple occupation states also contribute small but finite weights. While in the SAFM phase, the single, double and triple occupations with the same spin alignment, p , d and r , are dominant. The spin singlet and small spin states contribute very little. With increasing the Hund's rule coupling, the empty and single occupations continuously decrease, while the double and triple ones considerably increase. This behavior arises from the fact that the increase of Coulomb interaction favors the formation of the SAFM phase, and large Hund's rule coupling favors large spin state.

The gap opening behavior of the SDW states in the multi-orbital FeAs-based system is an interesting but unsolved topic. In order to resolve the behavior of the SDW gap opening in $K_xFe_{2-y}Se_2$, we present the band dispersions of the PM and SDW states in Fig. 6. We find that in the SDW

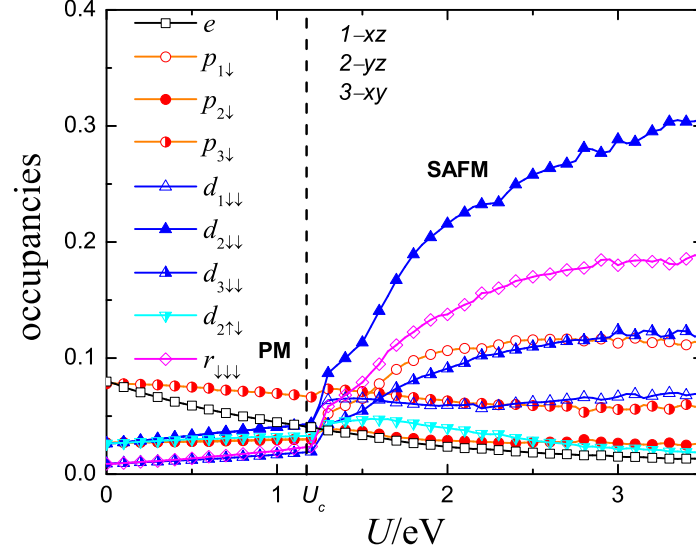


FIG. 5. Dependence of various boson occupancies on the Coulomb interaction U at $n=4$, and $J_H=0.25U$.

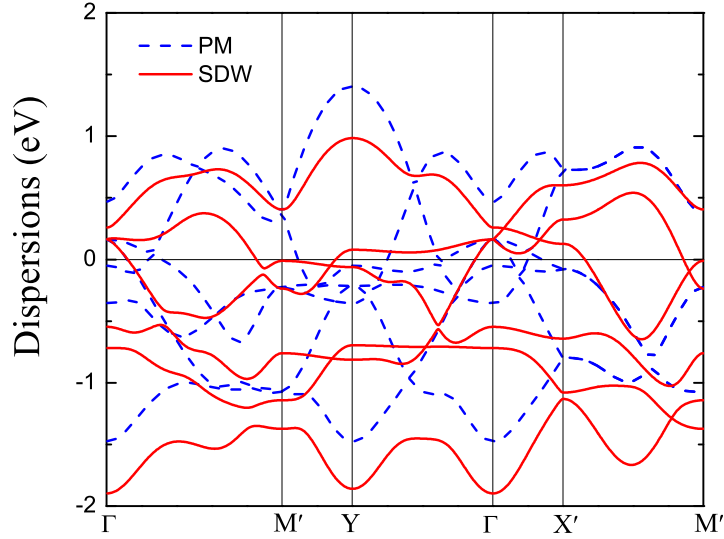


FIG. 6. Band dispersions of the PM and SDW states along the high symmetry points, Γ (0,0), Y (0, π), M' ($\pi/2, \pi$), X' ($\pi/2, 0$), in the folded BZ with $U=0$ and 2 eV, and $J_H=0.25U$ at $n=4$.

states, only partial SDW gaps open near E_F in comparison with PM states, which is the consequence of the the band narrowing and spin splitting, similar to FeAs-based compounds. The partial opening of SDW gap indicates the system is a bad metal.

The dependence of orbital occupations and magnetic moment of each orbital on the Coulomb interaction U is also shown in Fig. 7. With the increase of U , once the system enters the SAFM

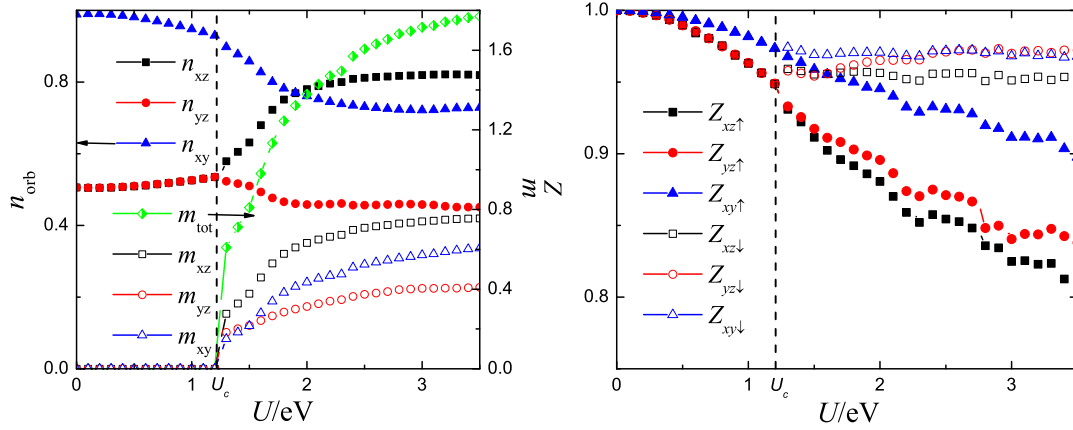


FIG. 7. (Color online) Dependence of orbital occupations and magnetic moment of each orbital (left panel), and renormalization factor (right panel) on the Coulomb interaction U at $n=4$, and $J_H=0.25U$.

phase, there is obvious orbital polarization between xz and yz orbitals together with $n_{xz} < n_{yz}$ in the electronic representation. And the magnetic moments on the xz and yz orbitals are different with $m_{xz} > m_{yz}$. These are consistent with the previous LaFeAsO results [21, 35]. The renormalization factors Z displayed in the right panel of Fig. 7 show that the $Z_{xz\uparrow}$, $Z_{yz\uparrow}$ and $Z_{xy\uparrow}$ become smaller and smaller with $Z_{xz/yz\uparrow} < Z_{xy\uparrow}$ when U increases. This indicates that the SDW gap opening mainly occurs in the xz/yz orbitals.

The evolution of the PDOS with Coulomb interactions U is also displayed in Fig. 8. We find that at $U=2.0$ eV and 3.0 eV, there exhibit obvious spin polarizations in SAFM phase due to the breakdown of spin symmetry. The xz - and yz - orbitals dominate the FS, while the xy orbital mainly lies far from the Fermi levels. This also shows that the xz/yz orbitals determine the electronic properties near E_F , and mainly involve with the formation of the SDW states, consistent with the result of renormalization factor in Fig. 7.

Since the electronic correlation is intermediate, one expects that U is larger than 2 eV in iron pnictides and selenides; thus at $2/3$ filling, the SAFM state with orbital ordering is stable over a wide electron correlation range, from intermediate to strong correlations, which is similar to the FeAs-based systems.

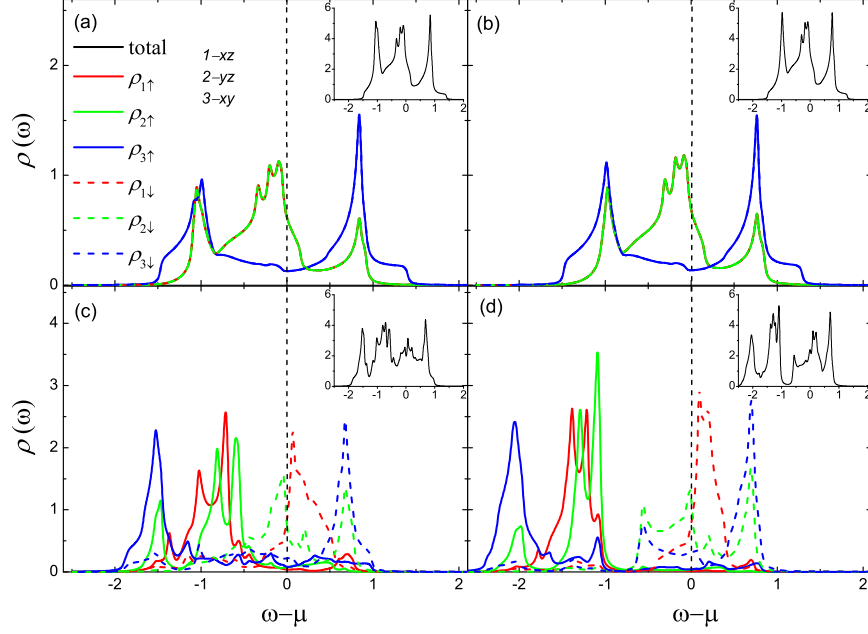


FIG. 8. Projected densities of states are plotted for $U=0$ (a), 1.0 eV (b), 2.0 eV (c), and 3.0 eV (d) at $n=4$, respectively, with $J_H=0.25U$. Inset: total densities of states.

C. Half-filling case

When turning to the half-filling case, which corresponds to the Fe^{3+} -based systems, such as KFeSe_2 and FeAs compounds, *etc.*, we find that the phase diagram becomes much richer. It is found that there exist three critical points when U increases: the system transits from a PM metal to an SAFM metal at U_{c1} , from an SAFM metal to a *Néel* AFM metallic phase at U_{c2} , and from an AFM metal with intermediate-spin state to an AFM OSMP with high-spin state at U_{c3} , as shown in Fig. 9. These phases will be addressed in detail in the following. In comparison with $n=4.5$ and 4 cases, we find that besides the PM and SAFM phases, the *Néel* AFM metallic phase appears in slightly large U region at $U_{c2} \approx 0.8$ eV. Only when in the narrow Coulomb interaction region at $U_{c1} \approx 0.65 < U < U_{c2}$, the SAFM phase is stable, as the dependence of the boson occupancies on Coulomb interaction U showing in Fig. 9. With the increase of the Coulomb interaction, the triple occupation $r_{\downarrow\downarrow\downarrow}$ sharply increases, while the other high occupations are relatively small. This shows that the system undergoes a spin state transition with the increase of the Coulomb interaction and the Hund's rule coupling, as we see the low-spin ($S=1/2$) to intermediate-spin ($S=1$) transition at U_{c2} in Fig. 10.

On the other hand, the dependence of the orbital occupations and the magnetic moments of

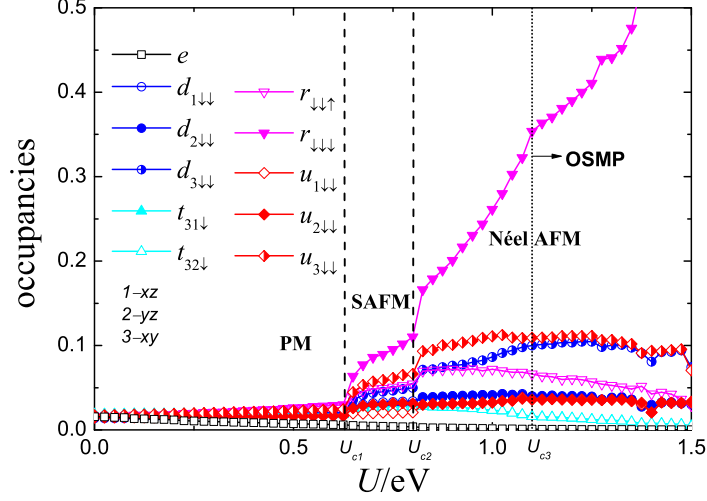


FIG. 9. Dependence of boson occupancies on Coulomb interaction U at half-filling $n=3$ and $J_H=0.25U$. Three dashed vertical lines denote the phase boundaries of the PM-SAFM, SAFM-Néel AFM, and Néel AFM-OSMP transitions at U_{c1} , U_{c2} and U_{c3} , respectively.

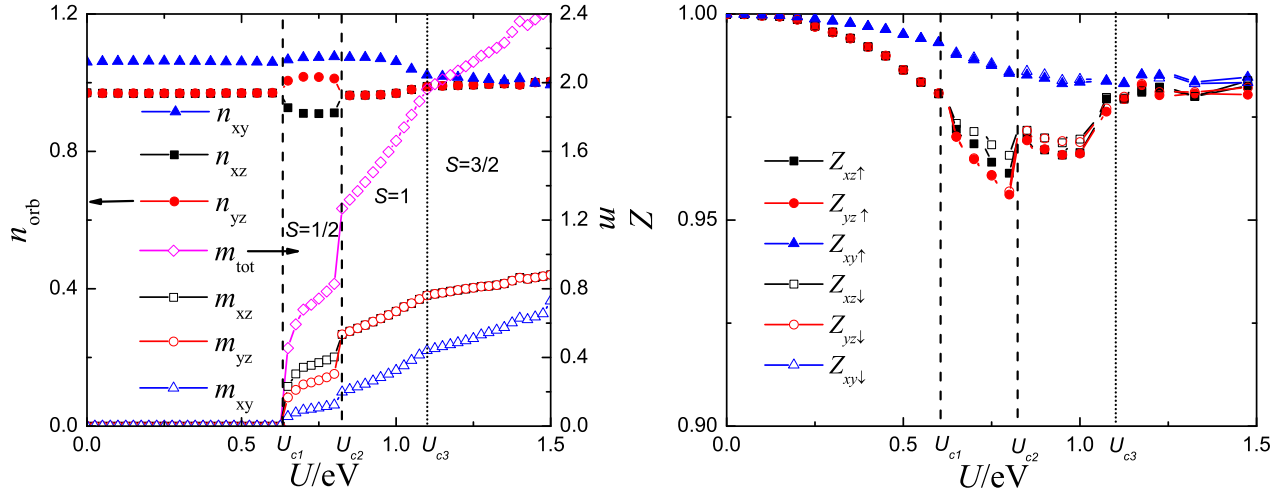


FIG. 10. (Color online) Orbital occupations and magnetic moment of each orbital (left panel), and renormalization factor (right panel) as a function of Coulomb interaction U at half-filling $n=3$, and $J_H=0.25U$. The dashed lines indicate the phase boundaries U_{c1} , U_{c2} and U_{c3} .

three orbitals on Coulomb interaction U is plotted in the left panel of Fig. 10. We find that in the SAFM phase, a small orbital polarization appears with $n_{yz} > n_{xz}$ in the present hole representation, *i.e.* $n_{xz} > n_{yz}$ in the electron representation. This supports the itinerant orbital ordering in the parent

phases of iron pnictides [23, 35]. Meanwhile the magnetic moments on different orbitals possess $m_{yz} < m_{xz}$ with total magnetic moment $m_{tot} < 1\mu_B$. The system lies in a low-spin state. However, in the *Néel* AFM metallic phase, there is no orbital polarization, since in the presence of the spin-orbital coupling, the preserved spin rotational symmetry does not lift the orbital degeneracy or break the orbital symmetry. When $U > U_{c3}$, the system enters the OSMP phase, as displayed in the left panel of Fig. 10. All of the three orbital occupations are nearly equal to 1. The magnetic moment per orbital steeply increases, and the total magnetic moment m_{tot} is larger than $2\mu_B$. Meanwhile, the system undergoes an intermediate-spin ($S=1$) to high spin ($S=3/2$) transition with the increasing of U , and thus enters a high-spin state when $U > U_{c3}$.

The right panel of Fig. 10 displays the renormalization factor of each orbital as a function of Coulomb interaction U , which is in sharp contrast with the $n=4.5$ and 4 cases. In the PM and SAFM phases, all the renormalization factors Z_{xz} , Z_{yz} and Z_{xy} ($Z_{xz/yz} < Z_{xy}$) smoothly decrease with increasing U , indicating the bandwidths become narrow due to the increase of the Coulomb correlation. When $U > U_{c2}$, the system enters the *Néel* AFM state. In this situation Z_{xy} gradually decreases, while Z_{xz} and Z_{yz} considerably change with U , suggesting that the variations of orbital and magnetic states mainly occur in these two orbitals. The lift of Z_{xz} and Z_{yz} implies the bandwidths of the two orbitals anomalously increase, which is attributed to the fact that the exchange splitting of spin-up and spin-down subbands of the xz - and yz -orbitals increases with the increase of U , leading to the total bandwidth broadening, which is also seen in Fig. 11 in what follows.

We present the PDOS of four typical phases, including PM, SAFM, *Néel* AFM metal and AFM OSMP, in Fig. 11 for Coulomb interaction $U=0, 0.75, 1.0$ and 1.5 eV, respectively. It is found that in relatively small U region, *i.e.* $U \leq U_{c2}$, the xz/yz orbitals dominate the FS in both the PM and SAFM phases. Different from Fig. 11(a), in the SAFM phase with $U=0.75$ eV in Fig. 11(b), the orbital degeneracy between xz and yz orbitals is lifted, consistent with the orbital polarization in the left panel of Fig. 10. Meanwhile in the *Néel* AFM metallic state with $U=1.0$ eV in Fig. 11(c), the weight of the xz and yz orbitals in the FS is greatly suppressed; but the spin splitting becomes large, consistent with the intermediate spin configuration in Fig. 10. Interestingly, we find that when $U > U_{c3} \approx 1.1$ eV, an orbital-selective Mott transition occurs, *i.e.* an OSMP emerges. In this situation, only the broad xy orbital contributes to the FS, while the narrow xz and yz orbitals are insulating and sank below the FS, as seen the PDOS with $U=1$ eV in Fig. 11(d).

Therefore, at a half filling, the system is mainly a *Néel* AFM state without orbital ordering in the intermediate and strong correlations, in addition to an OSMP phase related with an intermediate-

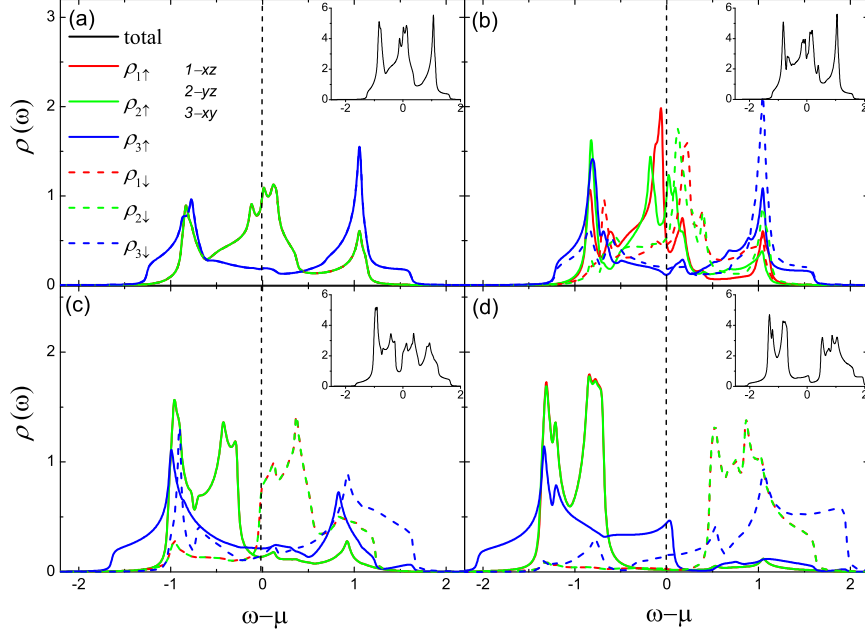


FIG. 11. Projected densities of states are plotted for $U=0$ (a), 0.75 eV (b), 1.0 eV (c), and 1.5 eV (d) at half-filling $n=3$, respectively. $J_H=0.25U$. Inset: total densities of states.

spin to high-spin transition. Compared with the other band fillings, the different magnetic phase diagrams suggest a band-filling controlling magnetism scenario in the iron selenide systems.

IV. DISCUSSION AND SUMMARY

The scenario of the orbital selective Mott transition in $K_x\text{Fe}_{2-y}\text{Se}_2$ could be understood in a sketch of OSMP in the presence of magnetism shown in Fig. 12 through tuning the band filling and the correlation strength. When tuning to the half-filling, with the increase of Coulomb interaction and Hund's rule coupling, the spin-up and spin-down subbands split with each other, and the spin-up xz - and yz -orbitals are filled, sank below E_F and become insulating; while the xy -orbital remains across E_F and is conducting, giving rise to an AFM OSMP. We notice that in comparison with the bandwidths of $K_x\text{Fe}_{2-y}\text{Se}_2$, the U_{c3} for the occurrence of the OSMP is small. This may arise from the following two reasons: (1) in the parent phase of Fe-based superconductors, the Hund's rule coupling is large with $J_H=0.25U$. If small values $J_H=0.15U$ or $0.1U$ are adopted, U_{c3} will reach a relatively large values up to 2 or even 3 eV; (2) U_{c3} is obtained for the OSMP with AFM order in the present study, it will become larger in the PM situation. Since $K\text{FeSe}_2$ possesses not only tetrahedra crystal field but also large magnetic moment, it may be a potential candidate for such an

OSMP phase. We expect that further increasing the Coulomb interaction U will drive the system to a magnetic insulating state accompanied with a metal-insulator transition.

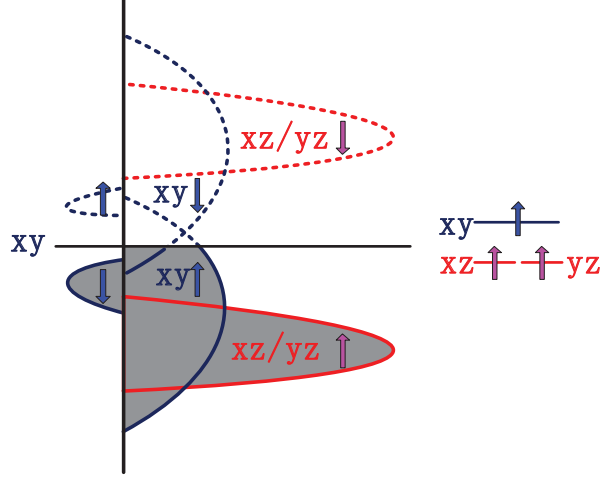


FIG. 12. Sketch of sublattice band structures in the orbital-selective Mott phase with *Néel* antiferromagnetism for half-filled three-orbital model in $\text{K}_x\text{Fe}_{2-y}\text{Se}_2$.

We notice that different from our PM results, the first-principles electronic structure calculations suggested the ground state in KFe_2Se_2 is the SAFM ordering [9], or the bi-collinear AFM ordering resulting from the interplay among the nearest, the next-nearest, and the next-next-nearest neighbor superexchange interactions mediated by Se $4p$ -orbitals in AFe_2Se_2 ($\text{A}=\text{K}, \text{Tl}, \text{Rb}, \text{or Cs}$) [8]. In addition, some other iron-based materials, such as FeSe [36, 37], LiFeAs [38], and KFe_2As_2 [38–40], *etc.*, have no magnetism at all as observed in the experiments, but AFM is obtained in the LDA calculations. The discrepancies among these materials suggest the magnetism is sensitive to the electronic properties or lattice distortion [38]. The LDA methods usually so overestimate the magnetic moment and AFM ordering but omit some spin fluctuations of the system due to the intermediate electronic correlation that a proper treatment on the electronic correlation in these FeSe -based compounds may be important for understanding its magnetic ground state. In our study, we deal with the electronic correlation within the framework of the KRSB approach which is verified as an effective approach to treat the electronic correlation ranging from weak through intermediate to strong ones. Our PM groundstate result, not non-magnetic one, indicates that there exists strong spin fluctuation which is regarded as the superconducting pairing mechanism, thus KFe_2Se_2 is a potential candidate of the parent phase for superconductor without doping. Moreover, a recent STS experiment demonstrated the existence of phase separation and distinguished

the contributions: the KFe_2Se_2 component contributes to superconductivity, while the $\text{K}_{0.8}\text{Fe}_{1.6}\text{Se}_2$ Fe-vacancy ordering component to the insulating properties [14], suggesting that pure KFe_2Se_2 is more possibly a PM phase when in the normal state. These observations are consistent with our present results.

In summary, starting with an effective three-orbital model for newly found KFe_2Se_2 , we have shown that the ground state of KFe_2Se_2 at three-quarter filling is a paramagnetic metallic phase. We also suggest a possible OSMF phase through tuning the band-filling in $\text{K}_x\text{Fe}_{2-y}\text{Se}_2$. Our results demonstrate that the band filling plays a key role in the electronic and magnetic properties of $\text{K}_x\text{Fe}_{2-y}\text{Se}_2$. Since the phase separation widely exists in $\text{K}_x\text{Fe}_{2-y}\text{Se}_2$ materials, future experiments are expected to confirm the magnetic ground state of KFe_2Se_2 . In addition, the influences of the band filling and correlation on the electronic structures and magnetic properties in the presence of Fe vacancies for $\text{K}_x\text{Fe}_{2-y}\text{Se}_2$ is an interesting topic, thus further theoretical works are expected.

ACKNOWLEDGMENTS

The author (D.Y.) gratefully acknowledge the help of Da-Mei Zhu with the manuscript. This work was supported by the Natural Science Foundation of China (NSFC) No. 11104274, 11074257, and of Anhui Province No. 11040606Q56, and the Knowledge Innovation Program of the Chinese Academy of Sciences. Numerical calculations were performed at the Center for Computational Science of CASHIPS.

-
- [1] J. G. Guo, S. F. Jin, G. Wang, S. C. Wang, K. X. Zhu, T. T. Zhou, M. He, and X. L. Chen, Phys. Rev. B **82**, 180520(R) (2010).
 - [2] M. H. Fang, H. D. Wang, C. H. Dong, Z. J. Li, C. M. Feng, J. Chen, and H. Q. Yuan, Europhys. Lett. **94**, 27009 (2011).
 - [3] Z. Wang, Y. J. Song, H. L. Shi, Z. W. Wang, Z. Chen, H. F. Tian, G. F. Chen, J. G. Guo, H. X. Yang, and J. Q. Li, Phys. Rev. B **83**, 140505(R) (2011).
 - [4] W. Bao, Q. Z. Huang, G. F. Chen, M. A. Green, D. M. Wang, J. B. He, X. Q. Wang, and Y. Qiu, Chin. Phys. Lett. **28**, 086104 (2011).

- [5] F. Ye, S. Chi, W. Bao, X. F. Wang, J. J. Ying, X. H. Chen, H. D. Wang, C. H. Dong, and M. H. Fang, Phys. Rev. Lett. **107**, 137003 (2011).
- [6] Y. Zhang, L. X. Yang, M. Xu, Z. R. Ye, F. Chen, C. He, H. C. Xu, J. Jiang, B. P. Xie, J. J. Ying, X. F. Wang, X. H. Chen, J. P. Hu, M. Matsunami, S. Kimura, and D. L. Feng, Nat. Mater. **10**, 273 (2011).
- [7] T. Qian, X. P. Wang, W. C. Jin, P. Zhang, P. Richard, G. Xu, X. Dai, Z. Fang, J. G. Guo, X. L. Chen, and H. Ding, Phys. Rev. Lett. **106**, 187001 (2011).
- [8] X. W. Yan, M. Gao, Z. Y. Lu, and T. Xiang, Phys. Rev. B **84**, 054502 (2011).
- [9] C. Cao, and J. H. Dai, Chin. Phys. Lett. **28**, 057402 (2011).
- [10] W. Bao, Y. Qiu, Q. Huang, M. A. Green, P. Zajdel, M. R. Fitzsimmons, M. Zhernenkov, S. Chang, M. H. Fang, B. Qian, E. K. Vehstedt, J. H. Yang, H. M. Pham, L. Spinu, and Z. Q. Mao, Phys. Rev. Lett. **102**, 247001 (2009).
- [11] L. J. Zhang, and D. J. Singh, Phys. Rev. B **79**, 094528 (2009).
- [12] D. Y. Liu, Y. M. Quan, Z. Zeng, and L. J. Zou, Physica B **407**, 1139 (2012).
- [13] T. A. Maier, S. Graser, P. J. Hirschfeld, and D. J. Scalapino, Phys. Rev. B **83**, 100515(R) (2011).
- [14] W. Li, H. Ding, P. Deng, K. Chang, C. L. Song, K. He, L. L. Wang, X. C. Ma, J. P. Hu, X. Chen, and Q. K. Xue, Nat. Phys. **8**, 126 (2011).
- [15] Y. J. Yan, M. Zhang, A. F. Wang, J. J. Ying, Z. Y. Li, W. Qin, X. G. Luo, J. Q. Li, J. P. Hu, and X. H. Chen, Sci. Rep. **2**, 212 (2012).
- [16] F. Chen, M. Xu, Q. Q. Ge, Y. Zhang, Z. R. Ye, L. X. Yang, J. Jiang, B. P. Xie, R. C. Che, M. Zhang, A. F. Wang, X. H. Chen, D. W. Shen, J. P. Hu, and D. L. Feng, Phys. Rev. X **1**, 021020 (2011).
- [17] C. H. Li, B. Shen, F. Han, X. Y. Zhu, and H. H. Wen, Phys. Rev. B **83**, 184521 (2011).
- [18] P. Cai, C. Ye, W. Ruan, X. D. Zhou, A. F. Wang, M. Zhang, X. H. Chen, and Y. Y. Wang, Phys. Rev. B **85**, 094512 (2012).
- [19] R. H. Yuan, T. Dong, Y. J. Song, P. Zheng, G. F. Chen, J. P. Hu, J. Q. Li, and N. L. Wang, Sci. Rep. **2**, 221 (2012).
- [20] A. M. Zhang, T. L. Xia, W. Tong, Z. R. Yang, and Q. M. Zhang, arXiv:1203.1533.
- [21] Y. M. Quan, L. J. Zou, D. Y. Liu, and H. Q. Lin, J. Phys.: Condens. Matter **24**, 085603 (2012).
- [22] G. Kotliar and A. Ruckenstein, Phys. Rev. Lett. **57**, 1362 (1986).
- [23] Y. M. Quan, L. J. Zou, D. Y. Liu, and H. Q. Lin, Eur. Phys. J. B **85**, 55 (2012).
- [24] P. A. Lee, and X. G. Wen, Phys. Rev. B **78**, 144517 (2008).
- [25] F. Krüger, S. Kumar, J. Zaanen, and J. van den Brink, Phys. Rev. B **79**, 054504 (2009).

- [26] S. L. Yu, J. Kang, and J. X. Li, Phys. Rev. B **79**, 064517 (2009).
- [27] M. Daghofer, A. Nicholson, A. Moreo, and E. Dagotto, Phys. Rev. B **81**, 014511 (2010).
- [28] S. Zhou, and Z. Q. Wang, Phys. Rev. Lett. **105**, 096401 (2010).
- [29] S. Graser, A. F. Kemper, T. A. Maier, H. P. Cheng, P. J. Hirschfeld, and D. J. Scalapino, Phys. Rev. B **81**, 214503 (2010).
- [30] M. L. Foo, Y. Y. Wang, S. Watauchi, H. W. Zandbergen, T. He, R. J. Cava, and N. P. Ong, Phys. Rev. Lett. **104**, 247001 (2004).
- [31] S. M. Huang, and C. Y. Mou, Phys. Rev. B **84**, 184521 (2011).
- [32] V. Brouet, M. Marsi, B. Mansart, A. Nicolaou, A. Taleb-Ibrahimi, P. Le Fèvre, F. Bertran, F. Rullier-Albenque, A. Forget, and D. Colson, Phys. Rev. B **80**, 165115 (2009).
- [33] H. Shishido, A. F. Bangura, A. I. Coldea, S. Tonegawa, K. Hashimoto, S. Kasahara, P. M. C. Rourke, H. Ikeda, T. Terashima, R. Settai, Y. Ōnuki, D. Vignolles, C. Proust, B. Vignolle, A. McCollam, Y. Matsuda, T. Shibauchi, and A. Carrington, Phys. Rev. Lett. **104**, 057008 (2010).
- [34] S. Raghu, X. L. Qi, C. X. Liu, D. J. Scalapino, and S. C. Zhang, Phys. Rev. B **77**, 220503(R) (2008).
- [35] D. Y. Liu, Y. M. Quan, D. M. Chen, L. J. Zou, and H. Q. Lin, Phys. Rev. B **84**, 064435 (2011).
- [36] F. J. Ma, W. Ji, J. P. Hu, Z. Y. Lu, and T. Xiang, Phys. Rev. Lett. **102**, 177003 (2009).
- [37] T. Imai, K. Ahilan, F. L. Ning, T. M. McQueen, and R. J. Cava, Phys. Rev. Lett. **102**, 177005 (2009).
- [38] Z. P. Yin, K. Haule, G. Kotliar, Nat. Mater. **10**, 932 (2011).
- [39] T. Sato, K. Nakayama, Y. Sekiba, P. Richard, Y.-M. Xu, S. Souma, T. Takahashi, G. F. Chen, J. L. Luo, N. L. Wang, and H. Ding, Phys. Rev. Lett. **103**, 047002 (2009).
- [40] C. H. Lee, K. Kihou, H. Kawano-Furukawa, T. Saito, A. Iyo, H. Eisaki, H. Fukazawa, Y. Kohori, K. Suzuki, H. Usui, K. Kuroki, and K. Yamada, Phys. Rev. Lett. **106**, 067003 (2011).